Extraction and analysis of elevation changes in Antarctic ice sheet from CryoSat-2 and Sentinel-3 radar altimeters

Song Li,[a,b] **Jingjuan Liao**,[a,*] **and Lianchong Zhang**[a]
[a]Chinese Academy of Sciences, Key Laboratory of Digital Earth Science, Aerospace Information Research Institution, Beijing, China
[b]University of Chinese Academy of Sciences, Beijing, China

Abstract. New radar altimeters have supported elevation modeling with greater accuracy and extended periods in recent years. Sentinel-3 has been rarely used in previous studies for monitoring the Antarctic ice sheet. The CryoSat-2 and Sentinel-3 satellite radar altimeter data were combined to extract the elevation changes in the Antarctic ice sheet. First, a subregional data filtering method based on a clustering algorithm was proposed to improve the accuracy of the elevation change results for the outliers in the original measurements. Next, an improved model-fitting model that incorporated multiple parameters was used to extract elevation changes, and the results were validated using airborne laser altimetry data and ICESat-2 data. The average changes in the Antarctic ice sheet elevation from 2016 to 2019 were -4.3 ± 0.9 cm/y. The elevation changes of the ice shelf edges with large slopes and complex topography were much larger than the interior. Some specific areas showed substantial elevation changes. The most significant surface decreases occurred at the Pine Island Glacier and the Totten Glacier, while a pronounced surface heightening existed at the Kamb Ice Stream. We reveal an effective method for combining Antarctic ice sheet data from new radar altimeters. This method supports the long-term monitoring of the Antarctic ice sheet and global climate change in the future. [DOI: 10.1117/1.JRS.16.034514]

Keywords: elevation changes; Antarctic ice sheet; satellite radar altimeter.

Paper 220213G received Apr. 8, 2022; accepted for publication Jul. 19, 2022; published online Aug. 2, 2022.

1 Introduction

The surface topography of the Antarctic ice sheet and its changes are closely related to polar and global climate changes. Therefore, monitoring elevation changes in the Antarctic ice sheet is essential to study the ice sheet's evolution and understand the response of Antarctica to climate change.[1] Previous studies have indicated that the melting of the Antarctic ice sheet has been accelerating in recent years,[2–4] which led to a global sea-level rise.[5] Furthermore, the melt-water-induced warming of the subsurface ocean could cause further melting of the ice sheet and shelves through a positive feedback mechanism, threatening humans living near the coast.[1,5]

Satellite altimetry is an effective way to monitor the polar ice sheet.[6] Satellite altimeters were first used to measure ice sheet elevations by Zwally et al. in 1983; surface elevations were contoured for the region of Greenland south of 72°N and for the region of East Antarctica north of 72°S covered by SeaSat.[7] During the last few decades, satellite radar altimeter data have provided almost complete and continuous coverage of the polar regions. These data supported studies related to the polar areas, including digital elevation model mapping of the ice sheet, long-term elevation changes estimation, and mass and volume changes.[8,9] For example, one study[10] used ERS-2 satellite data to analyze elevation changes in the Antarctic ice sheet between 1995 and 2000. Using ICESat data, another study[11] monitored elevation changes in the Antarctic ice sheet. These studies based on satellite altimeters showed that the most severe elevation decrease occurred in the West Antarctic, particularly in parts of the glaciers near the Amundsen Sea at a rate of 9 m/y.[11] In contrast, the elevation of the East Antarctic was largely stable.[12,13]

*Address all correspondence to Jingjuan Liao, liaojj@aircas.ac.cn

In 2014, McMillan et al. and Helm et al.[14,15] monitored the Antarctic ice surface elevation using CryoSat-2 data and obtained consistent conclusions.

Altimeter data for extracting elevation changes in ice sheets are continuously updated. Previous studies have combined different altimeter missions to achieve more effective long-term elevation changes monitoring. For example, Wingham[16] combined ERS-1 and ERS-2 satellite data to measure ice sheet elevation changes during 1992 to 2003, Li and Davis[17] combined ERS-2 and Envisat data to construct time series elevation changes in the interannual ice sheet, and Fricker and Padman[18] also used SeaSat, ERS-1/2, and Envisat to study ice shelf elevation changes. One of the critical issues in combining data acquired by various missions is bias correction. Paolo et al.[19] and Adusumilli et al.[20] established a time series of ice shelf elevation changes based on multiple missions after correcting for intermission bias. Meanwhile, Schröder et al.[21] used SeaSat, Geosat, ERS-1, ERS-2, Envisat, ICESat, and CryoSat-2 data to analyze a 40-year time series of ice sheet elevation changes.

The altimeters used in the above studies are operated in a closed-loop tracking mode, which cannot measure the correct tracking distance for abrupt topographic changes.[22] In contrast, a new radar altimeter, Sentinel-3, uses an open-loop tracking system operated in Delay Doppler mode over the entire ice sheet region, providing a resolution of 300 m along track. It can also acquire higher accuracy elevation measurements over the Antarctic ice sheet, the instrument achieves both an accuracy and a precision of the order of 10 cm over the low-slope regions of the ice sheet interior.[23] Considering that CryoSat-2 already has an overrun problem, Sentinel-3 altimetry data can provide a new data guarantee for Antarctic ice cap elevation monitoring, which is valuable for the study of long time series elevation change of the ice cap. Therefore, it is important to study the integration of Sentinel-3 and CryoSat-2, a fore-sequence altimeter.

The least-squares plane fitting method is widely used to extract ice sheet elevation variations, and multiple parameters can be included in the model simultaneously.[21,24–26] Based on the simple model depicting temporal and topographic variations, Wingham, Davis, and Zwally et al. incorporated backscatter coefficients to correct penetration depth variations caused by the electromagnetic properties of the ice sheet surface.[10,27,28] Flament and Rémy,[12] Simonsen and Sørensen,[26] and Michel et al.[29] added waveform parameters to the model. In addition, models that combine multiple data need to account for both the intermission bias and ascending-descending (A-D) bias between the two altimeter missions.[30] The two biases were treated separately in the above studies. However, Zhang et al. constructed a least-squares fitting model to correct the two biases simultaneously. They applied the model to Envisat and CryoSat-2 missions to analyze the Antarctic ice sheet's long-term elevation changes time series.[31] This model eliminated all biases simultaneously and was more suitable for the joint analysis of the two altimeter missions. The application in the fusion of Sentinel-3 data with previous altimeter data has not been carried out yet; therefore, the fitting model was used to monitor elevation changes in the Antarctic ice sheet combined with CryoSat-2 and Sentinel-3 data in this study. On the other hand, the outliers in the results obtained after the least-squares plane fitting are usually removed iteratively using the elevation difference at the crossovers through the 3σ outlier rejection criteria.[21,32] In this study, we combined clustering algorithms to optimize the data and reduce the error of the fitting calculations through the preliminary data filter.

In this study, the latest CryoSat-2 and Sentinel-3A satellite altimeter data were jointly used to analyze the surface elevation changes in the Antarctic ice sheet during 2016 to 2019. A subregional data filtering method based on a clustering algorithm was proposed to remove the outliers in elevation observations and improve the accuracy of fitting results. The elevation changes fitting model included corrections including linear time trend, topography, intermission bias, A-D bias, mode bias, backscatter, and waveform parameters. In this fitting model, the intermission bias was fused with the intramission bias, and both parts of the biases are corrected in a single calculation. The extraction results of the elevation changes were validated using Operation Ice Bridge (OIB) data obtained from laser altimeter and ICESat-2 Land Ice Height data and compared with previous results of elevation changes. The analysis was carried out based on the terrain of the ice sheet surface, including the relationship between surface elevation changes and topographic slope and the time series of elevation changes in different regions with different terrain features.

This study provides the latest data source and methodological support for Antarctic ice sheet elevation monitoring by validating the results of the joint application of Sentinel-3 and CryoSat-2. This provides a strong guarantee for studying the long time series of Antarctic ice sheet elevation changes. Meanwhile, the data filtering method of altimeter altimetry data proposed in this study improves the consistency of original altimetry measurements and the accuracy of subsequent model fitting. The fitting model of elevation change effectively combines two kinds of altimeter data, which is helpful for the fusion method of multisource altimeter data

2 Materials and Methods

2.1 *Data*

The altimetric data used to extract the elevation changes in this study are derived from the radar altimeters Cryosat-2 and Sentinel-3, and the validation data are divided into high-precision airborne laser altimetry data from the OIB Airborne Topographic Mapper (ATM) and ICESat-2 satellite-based laser altimetry data. Each of the data is described below.

2.1.1 *Satellite radar altimeter data*

CryoSat-2 was launched in April, 2010, and is still in orbit. It has an orbital altitude of 717 km, with a 369-day fully repeating orbit and a 30-day subperiod. It can extend its coverage to a latitude of 88 deg and has high data coverage at the edge of the ice sheet through a narrower orbital spacing.[33] Its primary payload is a synthetic aperture interferometric radar altimeter (SIRAL) with three measurement modes. There is a low-resolution mode (LRM) operated in the inner region of the Antarctic ice sheet and an interferometric mode (SARIn) used in the edge region. This mode is suitable for continuous observation of steep and complex edges of the ice sheet margin and large glaciers with rapid elevation changes. In addition, it can improve the ground resolution along the orbit to about 300 m.[34,35] CryoSat-2 L2I level products from January, 2016, to December, 2019, were used in this study. These data were LRM observations retracked by the OCOG (Offset Center of Gravity) retracker and SARIn observations retracked by the Wingham/Wallis model-fitted retracker. The L2I level products provided additional waveform parameters than the L2 level products.[36]

Because the operation of CryoSat-2 is currently beyond its lifetime, the latest on-orbit Sentinel-3 (delayed Doppler radar altimeter) will be an essential altimeter for measuring long-term ice sheet changes. Sentinel-3 has an orbital altitude of ∼830 km with a 27-day repeat period 4-day subperiod, and its primary payload is the Sentinel-3 Ku/C Radar Altimeter (SRAL).[37] Sentinel-3 is the first altimeter with high-resolution measurements throughout the ice sheet's interior. It has an on-orbit resolution of ∼350 m and a cross-orbit resolution of 1.6 to 3 km.[23] The Sentinel-3A L2 level terrestrial product, processed by various correction and retracking from March, 2016, to December, 2019, was used to construct the model in this study and provided elevation measurements, correction values, and multiple parameters processed by different methods. To improve the fusion of the data and the consistency of the results, the CryoSat-2 LRM and Sentinel-3A elevation measurements used in this study were the retracking products using OCOG. We clipped and extracted the two kinds of altimeter data to obtain geographical locations, elevation values, time records, backscatter coefficients, and waveform parameters while removing the observations with obvious quality problems.

Both radar altimeter data provide support for monitoring Antarctic ice sheet elevations. CryoSat-2 provides greater coverage of the Antarctic ice sheet than Sentinel-3, so elevation measurements south of 81.25 deg near the pole are provided by CryoSat-2 alone in joint applications. The high accuracy of the two altimeter data differs in different regions of the ice sheet. Sentinel-3 is able to provide higher accuracy measurements over a large area of the flat interior of the ice sheet, which is advantageous compared to CryoSat-2 LRM mode altimetry, while CryoSat-2 SARIn mode provides a significant improvement in accuracy over Sentinel-3 in complex edge regions. As a recently launched altimeter satellite, Sentinel-3 can play an important role in the long-term monitoring of the Antarctic ice sheet, replacing the earlier radar altimeter satellites.

2.1.2 *Validation data*

The results were validated using the airborne LiDAR altimetry data from the OIB and ATLAS/ICESat-2 L3A Land Ice Height (ATL06) data to assess the accuracy of our observed elevation changes. OIB has been continuously observing the North and South Poles since 2009. The payload of OIB in the Antarctic region is the ATM, and its vertical accuracy of the ATM elevation measurements can reach 7 ± 3 cm.[38] The ATML4 surface change in elevation data was composed of surface elevation change products for polar regions. It was used for the Antarctic ice sheet, including the change in elevation data from 2012 to 2016 and 2014 to 2016.[39] ATL06 data derived from ICESat-2. It provided geolocated estimates of land-ice surface heights and ancillary parameters that could be used to interpret the estimates and assess their quality.[40] The spatial resolution of the data was 20 m, and the selected time range was from October, 2018, to December, 2019.

The reasons for the selection of these validation data include both high measurement accuracy and temporal consistency. The necessity of OIB ATM data as validation data is its high accuracy. Since it is difficult to obtain actual measurement data in the Antarctic ice sheet, the ATM airborne altimetry data provide an approximation of the Antarctic ice sheet actual elevation measurements, which is important for the validation of the results of this study. However, the time range provided by OIB ATM data is different from the results of this study. ICESat-2 altimetry data compensate for the temporal consistency of the results, and they cover the entire Antarctic ice sheet with high resolution and accuracy, allowing for effective validation of the results of this study.

2.2 *Methods*

The main methods proposed and used in this study are the altimetric data filtering method and the elevation changes extraction method. The data filtering method is a subregional processing based on clustering algorithm, which aims to remove the outliers and improve the accuracy of subsequent model fitting. The elevation change extraction method is based on the least squares fitting model to achieve effective joint application of the two altimeter data. The following section describes in detail the specific parameter settings and steps of the data filtering method, as well as the construction of the fitting model and the extraction steps.

2.2.1 *Altimeter data filtering*

Due to the influence of the system errors from the altimeter and surface topography of the ice sheet, there are deviation values in the original elevation measurements from the satellite altimeter, leading to outliers in the extracted elevation changes. In previous studies, the outliers of elevation changes were often removed using the 3σ outlier rejection criteria after fitting the elevation changes[7,12] or by iterative computing the differences at the crossovers to remove the inconsistent values.[31,32] Instead of relying on postprocessing, this study presents a clustering algorithm and regional differences method to filter the original altimeter data before fitting the elevation changes. This method can remove the outliers from the altimetric data and ensure the accuracy of the data subsequently involved in model fitting, thus effectively improving the accuracy of the extracted elevation changes.

The K-means algorithm originates from a vector quantization method in signal processing. The purpose is to divide n points (a single observation or an instance of a sample) into k clusters. Each point belongs to the cluster corresponding to the nearest mean (i.e., cluster center), which is used as the criterion for clustering. The body of the algorithm is that the set of observations $(x_1, x_2, \ldots, x_n)$ is known and the K-means clustering is to divide these n observations into k sets ($k \leq n$) such that the sum of squares within-cluster is minimized.[41] That is, finding the clusters S_i that satisfy the following equation:

$$\arg \min_{S} \sum_{i=1}^{k} \sum_{x \in S_i} \|x - \mu_i\|^2. \tag{1}$$

where μ_i is the mean of all points in S_i.

Table 1 Parameters for different regions according to surface slope in the filtering method.

	Number of clusters (k)	Rejection condition	Termination condition
Low-slope region (<1.5 deg)	3	$d > 30$ m and $n < 1/3\, n_{max}$	$n < 30$ || ($d <= 30$ m||$n > 1/3\, n_{max}$)
High-slope region (>1.5 deg)	4	$d > 45$ m and $n < 1/3\, n_{max}$	$n < 30$ || ($d <= 45$ m||$n > 1/3\, n_{max}$)

In this study, elevation changes were calculated by gridding, and the measured elevation values within each grid were not uniform. It was normal to have some differences between the elevation measurements considering the undulations of the ice sheet topography and the different nature of the surface within the grid.[6] The topography of the Antarctic ice sheet is complex. The flatness of the interior and the steepness of the edge have different tolerances between measurements within the grid. Therefore, a subregional method was used in the data filtering. The grids were divided into low-slope regions (<1.5 deg) and high-slope regions (>1.5 deg) according to the local surface slope, and the classification determined the number of clusters k in the K-means clustering and the conditions in the selection. The specific steps of the method were:

- First, starting with a grid in the gridding study area and the parameters according to the slope of the grid were selected. Then, the measurements were clustered in range with K-means, and the number of measurements in range was counted as n.
- Second, the cluster with the largest n was selected, and the number of measurements in that cluster was counted as n max. Finally, the distance d between the center of the remaining clusters and the center of the largest cluster was calculated.
- Third, if a cluster met the rejection condition, the measurements were removed; if the termination condition was reached for all clusters, all the measurements were retained.
- Fourth, the above steps were iterated for the low-slope grids until the termination condition was met; only one cycle of filtering was performed for the high-slope grids.

The filtered measurements within this grid were obtained, and the filtering continued with the next grid. The parameters for the different slopes of regions are shown in Table 1.

2.2.2 *Elevation changes extraction*

The plane fitting method is widely used in extracting time series of ice sheet elevation changes.[12,21,24,25,42] This method can effectively separate signals from the topographic and ice-sheet changes in repeat-track altimetry data and accurately calculate the elevation changes from the ice sheet. The fitting model used in this study is first derived from the model proposed by Simonsen and Sørensen,[26] which considers the unaligned measurements in the short repetition cycle of CryoSat-2, the bias at the junction of the LRM and SARIn modes. Hence, the model includes the LRM and SARIn mode-bias and the A-D bias. In addition, seasonal variation and penetration variations, including backscatter coefficient (bs) and the waveform leading-edge width (lew), are added for correction. The model can be expressed as

$$\begin{aligned} h_i = {} & h_0 + dh/dt(t_i - t_0) \\ & + a_0 + a_1(x_i - x_0) + a_2(y_i - y_0) + a_3(x_i - x_0)^2 + a_4(y_i - y_0)^2 + a_5(x_i - x_0)(y_i - y_0) \\ & + dBS(bs_i - bs_0) + dLew(lew_i - lew_0) + \alpha \cos(\omega t_i) + \beta \sin(\omega t_i) + b_{AD}(-1)^{AD} \\ & + b_m(-1)^m + res. \end{aligned} \tag{2}$$

where $((x_i, y_i))$ and t_i are the coordinates and recording time of the measurements, respectively, t_0 is the reference time, h_i is the measured elevation at a given time and space, h_0 is the mean elevation at the grid centroid (x_0, y_0) used for least-squares fitting, $a_0 - a_5$ are the model parameters describing the local terrain, bs and lew are the backscatter coefficient and the waveform leading edge width, respectively, $\alpha \cos(\omega t_i) + \beta \sin(\omega t_i)$ is the seasonal variation term,

$b_{\mathrm{AD}}(-1)^{\mathrm{AD}} + b_m(-1)^m$ indicates the A-D bias and mode bias, and the values of AD and m are 1 (ascending/LRM mode) or 0 (descending/SARIn mode), and res is the residual.

The intermission and A-D biases exist between satellite altimeter missions.[43] The method of combining the two altimeters in this study refers to Zhang et al.,[31] incorporating the two biases in one least-squares fitting model. In addition, the data products used in this study contain waveform parameters, so the leading edge width of the waveform is also incorporated in the model, and the intermode bias $b_m(-1)^m$ is retained. The overall model is expressed as

$$\begin{aligned} h_i = {} & h_0 + dh/dt(t_i - t_0) \\ & + a_0 + a_1(x_i - x_0) + a_2(y_i - y_0) + a_3(x_i - x_0)^2 + a_4(y_i - y_0)^2 + a_5(x_i - x_0)(y_i - y_0) \\ & + dBS(bs_i - bs_0) + dLew(lew_i - lew_0) + \alpha \cos(\omega t_i) + \beta \sin(\omega t_i) \\ & + CS + b_m(-1)^m + res, \end{aligned} \tag{3}$$

where CS is the bias between CryoSat-2 and Sentinel-3 missions, denoted as

$$\begin{cases} CS = b_{C_aC_d}(-1)^{C_aC_d} + b_{C_aS_a}(-1)^{C_aS_a} + b_{C_aS_d}(-1)^{C_aS_d} + b_{C_dS_a}(-1)^{C_dS_a} + b_{C_dS_d}(-1)^{C_dS_d} \\ + b_{S_aS_d}(-1)^{S_aS_d} \\ b_{C_aS_a}(-1)^{C_aS_a} - b_{C_aS_d}(-1)^{C_aS_d} - b_{C_dS_a}(-1)^{C_dS_a} = 0, \\ b_{C_dS_d}(-1)^{C_dS_d} - b_{C_dS_a}(-1)^{C_dS_a} - b_{S_aS_d}(-1)^{S_aS_d} = 0, \\ b_{C_aS_d}(-1)^{C_aS_d} - b_{C_aC_d}(-1)^{C_aC_d} - b_{C_dS_a}(-1)^{C_dS_a} - b_{S_aS_d}(-1)^{S_aS_d} = 0, \end{cases} \tag{4}$$

where $b_{C_aC_d}(-1)^{C_aC_d}$ and $b_{S_aS_d}(-1)^{S_aS_d}$ are the A-D bias of CryoSat-2 or Sentinel-3, respectively, and $b_{C_aS_a}(-1)^{C_aS_a}$, $b_{C_aS_d}(-1)^{C_aS_d}$, $b_{C_dS_a}(-1)^{C_dS_a}$, and $b_{C_dS_d}(-1)^{C_dS_d}$ are the total biases of A-D bias and intermission bias between CryoSat-2 and Sentinel-3.

The specific forms of Eq. (3) and Eq. (4) in different grids are: if there is only LRM data in the grid, $b_m(-1)^m$ is 0 and CS contains only $b_{C_aC_d}(-1)^{C_aC_d}$; if there are two kinds of data (Sentinel-3+ CryoSat-2 LRM or Sentinel-3+CryoSat-2 SARIn), $b_m(-1)^m$ is 0; if there are three kinds of data (Sentinel-3+LRM+SARIn), all items in Eq. (3) are present.

We extracted the change in elevation rate based on the above: first, we gridded the study area according to the projection coordinates for data filtering. Here, we chose a resolution of 2.5 km × 2.5 km, and the grid containing more than 40 measurements was filtered by the method described in Sec. 2.2.1. Then, the measurements within a radius of 2.5 km around the grid centroid were used for filtering in this grid, and those grids containing more than 30 measurements were subjected to least-squares fitting according to Eq. (3). The elevation time variation of the calculable grid centers was extracted, and the outliers in fitting results were removed after each iteration using the 3σ outlier rejection criterion. The size of the grid and the selection of the interpolation method would affect the final fitting results.[44] Considering the computational efficiency and the accuracy of the results comprehensively, we chose the 5 km grid size and the Kriging interpolation method. Postprocessing was performed on the elevation changes to obtain the final elevation change time series of the Antarctic ice sheet at 5 km resolution. We used a median filter with a radius of 10 km to remove the outliers in the elevation change results. If there were <10 elevation rates in a 10-km radius, the radius was gradually expanded at 5 km intervals to 25 km.[21,45] Finally, the change trend and characteristics were derived.

3 Results and Discussion

In this study, the elevation change series of Antarctic ice sheet was constructed and the related validation and analysis were carried out. First, the validation of the results includes the validation of accuracy using OIB ATM data, the validation of the effect of the joint application of Sentinel-3 and CryoSat-2, and the validation of the accuracy using ICESat-2 data. Then, the elevation changes of the Antarctic ice sheet from 2016-2019 were analyzed, including the overall change analysis and the local change analysis in different geographical regions.

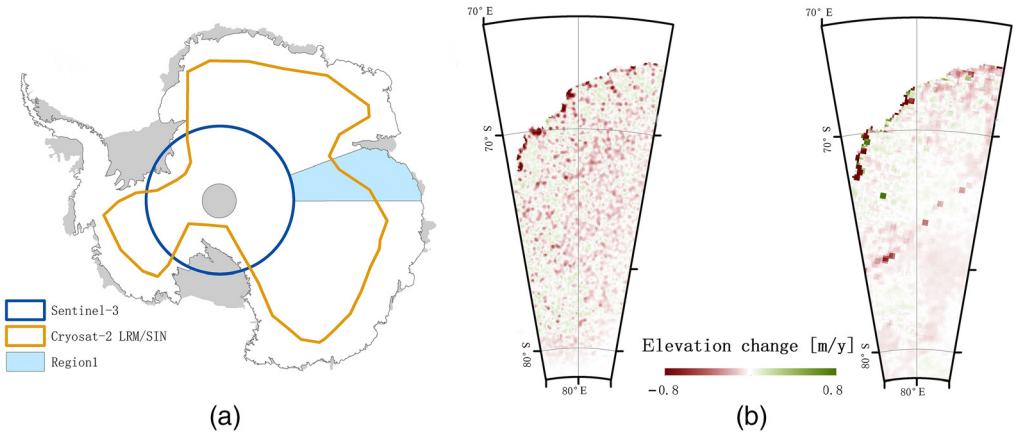

Fig. 1 (a) The mask boundaries of Sentinel-3A, CryoSat-2 LRM, and SARIn. (b) Comparison of filtering and no filtering results.

3.1 *Effect of the Data Filtering Method*

The purpose of data filtering was to remove those measurements with large deviations to avoid them causing outliers in the fitting results. If all original measurements are involved in the model fitting, outliers in results will occur at specific regions, including the junction of the two missions, the junction of the two modes, and the edge of the ice sheet with large topographic undulations. Figure 1(a) shows the mask boundaries of Sentinel-3, CryoSat-2 LRM, and SARIn, and region1 is selected as the study area to compare the effect of the data filtering method. The region1 is between 70° and 90°E and contains the Dome A, the American Highland, and the Wilhelm II Coast of the East Antarctic ice sheet. The ice sheet here is generally stable, and there is little difference between the marginal and internal changes, with rapid thinning only in some small areas. The region contains both the intersection of Sentinel-3A and LRM and the overlap of Sentinel-3A and SARIn data, demonstrating the applicability of this study's filtering method to different data combinations.

All the original measurements and the measurements processed by the data filtering were fitted separately using the method in Sec. 2.2.1. The percentage of data exclusions differed between regions after data filtering. Data for ice sheet areas with slopes > 1.5 deg were filtered to retain about 87% of the original data, and about 84% were retained for areas with small slopes. There was little difference in the percentage of data filtered between the two regions. Still, the number of original valid data on the lower slopes was significantly greater, and therefore more data were removed than on the higher slope regions. The surface change in elevation rates of region1 is shown in Fig. 1(b). The unfiltered results had a large average rate and had apparent patches. The elevation changes shown in the left figure are not continuous in a particular distribution. The elevation changes at the edges were much scattered, which is not in line with the actual situation of constant regional changes. The reason is that there were outliers in the unfiltered data. Once the number of outliers within the grid occupied a particular proportion, it led to fitting abnormal values. Due to the greater differences between the measurements at the edge of the ice sheet caused by the greater terrain undulation, more pronounced elevation changes were often obtained. In contrast, the results of the filtered measurements had a more continuous and smooth distribution of elevation changes, which generally showed a small change in the inland, a large change at the edge, and a trend of rapid lowering in some areas [see the right figure of Fig. 1(b)].

The statistics of the unfiltered and filtered results in different regions were compared in this study, and the means and standard deviations (STD) of each region are shown in Table 2. The result of LRM+S3 was better than that of SARIn+S3, the difference is mainly due to the different coverage of data. As shown in Fig. 1(a), the LRM runs on the flat interior of the ice sheet, while SARIn covers the complex margin, and the two differ greatly in terms of the terrain they cover. The accuracy of altimetry values is significantly better in the interior than at the margin, so despite the improved accuracy of the SARIn mode, the results were still worse than the interior

Table 2 Statistics of elevation changes obtained using unfiltered and filtering measurements in different regions.

	Unfiltered		Filtered	
Region	Mean (m/y)	STD (m/y)	Mean (m/y)	STD (m/y)
LRM+S3*	−0.048	0.105	−0.019	0.043
SARIn+S3*	−0.079	0.738	−0.024	0.223
Slope >1.5 deg	−0.187	0.978	−0.199	0.922
Totten Glacier	−2.125	0.803	−2.214	0.490

*There are two types of data coverage patterns: the LRM overlaps with Sentinel-3A and the SARIn overlaps with Sentinel-3A.

area measured by LRM. In the first two rows, the mean change in elevation rates of the unfiltered and filtered results did not differ much, and both had a general trend that the marginal changes were larger than the internal ones. However, by comparing the STD, the unfiltered STD was about three times bigger than the filtered results. The difference indicated that the elevation changes present better consistency and stability after data filtering, which was very important for the continuity of changes in large areas and the fitting of the whole Antarctic ice sheet. Two representative regions with large elevation changes were selected for comparative analysis to illustrate the performance of the data filtering algorithm in areas with significant elevation changes. The first region was the area with a slope > 1.5 deg. As shown in Table 2, there was a slight decrease in STD after data filtering, but the difference was not significant. This difference was due to the poor consistency of the altimetric measurements caused by the complex topography. Slight differences in the number of samples of several clusters were obtained after clustering. The number of effective altimetric measurements was initially relatively small, most of which were difficult to reach the filtering threshold. So only the individual extreme anomalies were removed, and the distribution characteristics of the original data were retained. Another region was the Totten Glacier, with significantly lower elevations. Despite the relatively large internal variation in the original measurements, the vast majority of the data showed a consistent decreasing trend. Therefore, the STD was reduced by about half after filtering, indicating that the filtering algorithm could improve the region with significant elevation changes.

3.2 *Comparison and Validation of the Elevation Changes Result*

The results in this study were first compared with the Antarctic elevation change results of 2012 to 2016 with a resolution of 5 km studied by Shepherd et al.[46] Thus, the elevation change difference in recent years was analyzed. Figure 2(a) shows a map of the difference between the 2016 to 2019 changes in this study and the 2012 to 2016 changes, reflecting a difference between the two periods. The results of this study are consistent with those of Shepherd et al. with an average elevation change rate difference of -0.98 ± 0.03 cm/y, which contains errors from processing methods, altimetry itself, and the accelerated ice sheet thinning due to global warming in recent years.[33] There is a small acceleration of ice sheet thinning in most of the Antarctic interior, and the difference between the two is mainly located at the edge. The apparent discrepancy regions can be divided into two types. One is the mountainous area near the Antarctic Peninsula and the Ross Sea, mainly attributed to the limited measurement accuracy of the altimeter and higher error rate of the fitting model in complex terrain areas. The other is the region reflecting the accelerated elevation change phenomena, such as Pine Island Glacier, where a more rapid ablation occurred in 2012 to 2016.

This study used the laser altimetry L4 elevation change data collected from the ATM in the OIB to validate the ice sheet change in elevation results. The validation data were distributed in the three regions represented by blue, yellow, and green in Fig. 2(b). The number of validation points in the three regions was 6344, 8361, and 40,385, respectively. The difference between the results of this study and the OIB data and the difference between the results of Shepherd et al.

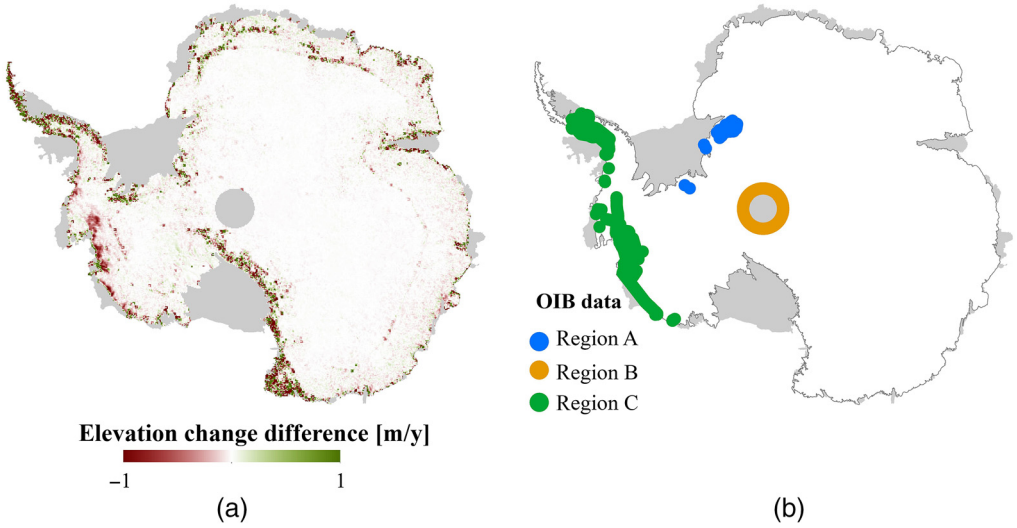

Fig. 2 (a) Difference between the 2016 to 2019 elevation changes from this study and the 2012 to 2016 elevation changes from Shepherd et al. (b) Distribution of OIB data points for validation.

and the OIB data were compared, counting the mean and root mean square error (RMSE) of the three validation regions separately (Table 3). As seen in Table 3, the change in the elevation rate of region B, which is inland, was significantly smaller than regions A and C. This validation data set had the smallest difference between the two study results. Region C, which included the Amundsen Sea shelves with the fastest lowing rate and the Antarctic Peninsula with large terrain undulation, had the largest difference with the OIB validation data. In region C, the RMSE of the two results was similar despite the differences in data source and time. This phenomenon may be due to the inherently high variability between data caused by the complex topography of region C. The large RMSE was not greatly affected despite the filtering and fitting processing. The statistics of all three regions showed that the differences between the results of this study and the OIB data were greater than those of Shepherd et al., due to the better time consistency of the latter and the accelerated thinning of the Antarctic ice sheet in the last 4 years. The correlation analysis in the three validation regions was performed separately to illustrate further the relationship between this study's results and the OIB data. The left three maps in Fig. 3 indicate the differences between the two data, where the yellow points represent the points with the difference in the range of -0.1 to 0.1 m/y and the blue and red points are points with a difference >0.1 m/y. The points in the three regions are mainly yellow, which indicates that the most elevation changes were very similar to the OIB data. Since regions A and C were located on the edge of the ice sheet, there were few points with large errors. The three scatter plots on the right side of Fig. 3 represent the relationship between the two data in the three regions. The accuracy of the OIB data was higher, so the distribution of the elevation change rates in this study was more scattered in Fig. 3. In the scatter plots, most points are concentrated in the yellow position, and the point on the red line indicates that the error between the result and the OIB data is 0. Although region C has the most dispersed distribution, the yellow areas of the three pictures are concentrated near the red line. This shows that the results of most points had slight

Table 3 The difference between the results of this study and OIB validation data and between the results of Shepherd et al. and the OIB validation data.

		Region A	Region B	Region C
This study	Mean (m/y)	0.021	0.015	−0.528
	RMSE (m/y)	0.203	0.095	0.981
Shepherd et al.	Mean (m/y)	0.017	0.016	−0.322
	RMSE (m/y)	0.211	0.084	0.994

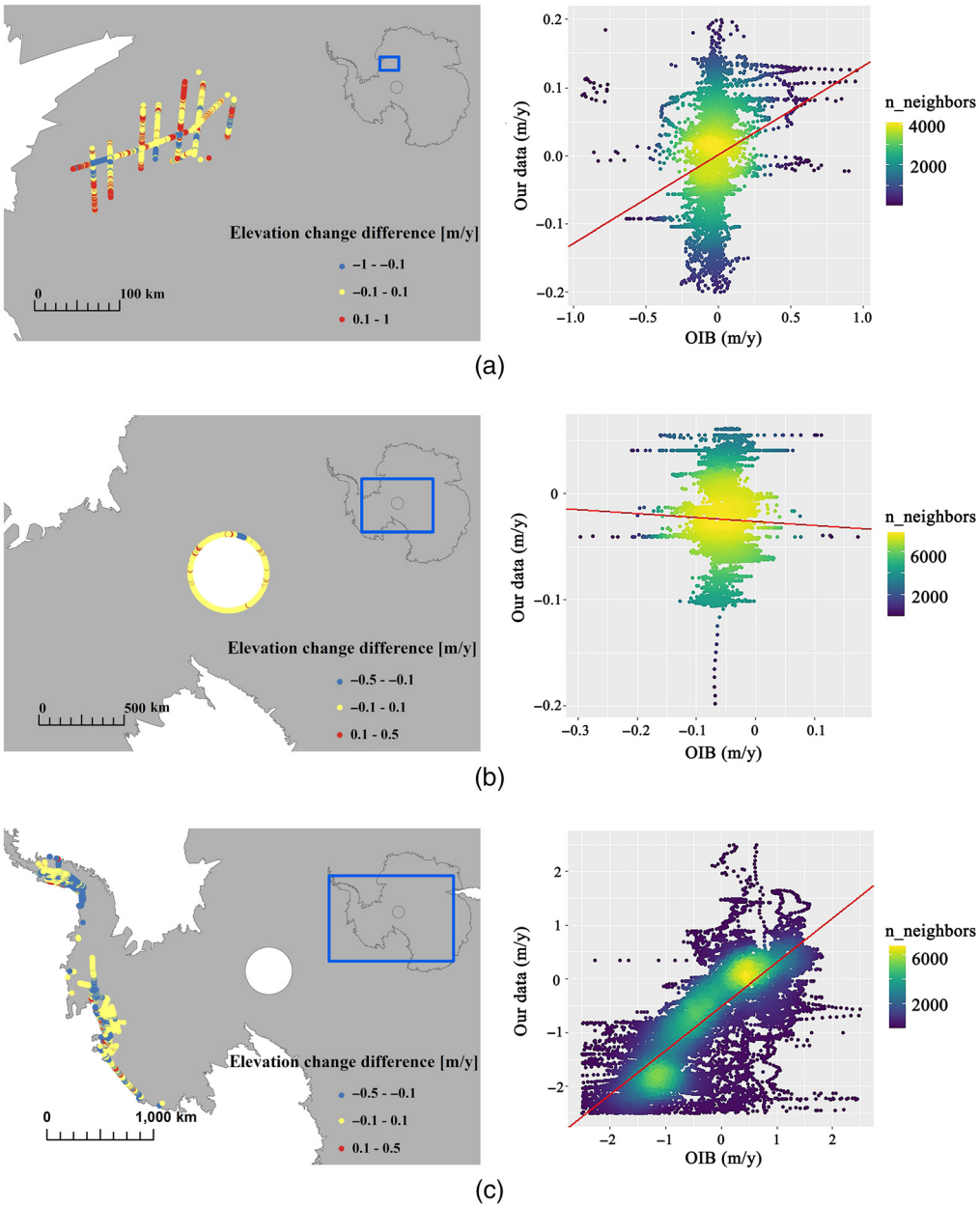

Fig. 3 Differences and scatter plots of the results of this study and OIB validation data. (a), (b), and (c) correspond to the validation region A, B, and C in Fig. 2(b), respectively, the left figures are graded differences between the two data, and the right figures are scatter plots of them.

differences from the validation data. These scatter plots are a more intuitive display of the left maps.

To verify whether the elevation change rates fitted jointly with the new radar altimeter data Sentinel-3 and CryoSat-2 have similar or better accuracy, a comparative analysis was conducted in this study for the elevation change rates extracted using CryoSat-2 only and that extracted jointly with the two data. Using the OIB ATM elevation measurements as validation data, validation points within region A and region C in Fig. 2(b) were selected, representing three different combinations of data patterns and different slope ranges, respectively (Table 4). For the ATM validation data and the CryoSat-2 altimeter data alone, the centroid values for the 2.5-km radius range were fitted according to the method used to extract the elevation change rates in this study, and the two elevation change rates with the same 5 km resolution were obtained as controls.

Using the elevation change rates extracted from the ATM elevation data as validation, the differences between the elevation change rates extracted using only CryoSat-2 and

Table 4 Comparison of accuracy of elevation change rate extracted before and after adding Sentinel-3 data.

Slope	Data	Mean (m/y)	RMSE (m/y)
<0.5 deg	LRM+S3	0.015	0.200
	LRM	0.019	0.205
<0.5 deg	SIN+S3	0.018	0.237
	SIN	0.020	0.221
>0.5 deg	SIN+S3	−0.403	0.764
	SIN	−0.399	0.750

Sentinel-3+CryoSat-2 and the validation data are counted separately (Table 4). It can be seen that the combined use of Sentienl-3 and CryoSat-2 improves the accuracy of the elevation change rates for the flatter interior ice sheet, with the mean difference reduced from 0.019 to 0.015 m/y. The same improvement is observed for the flatter edge region, with the mean differences reduced by 0.002 m/y. This demonstrates the reliability of the method and the significance of the combined use of Sentinel-3 and CryoSat-2 data.

This study further validated the results using ICESat-2 Land Ice Height data from October, 2018, to December, 2019, to meet the temporal consistency between the validation and altimeter data. Figure 4 shows the difference between our results and the ICESat-2 change in elevation rates. In the flat interior of the ice sheet, the difference was very small, almost an area <0.1 m. ICESat-2 has a higher measurement accuracy than satellite radar altimeters, especially at the edge of ice sheet and in areas with complex terrain. However, the most significant difference still exists in areas with drastic elevation changes and areas with complex topography. For example, the change in elevation rates from ICESat-2 was bigger than our change in elevation rates in Pine Island Glacier, and the difference in mountainous areas varied widely. Nevertheless, the differences in individual regions do not affect the consistency of the majority of the ice sheet region with the ICESat-2 validation data.

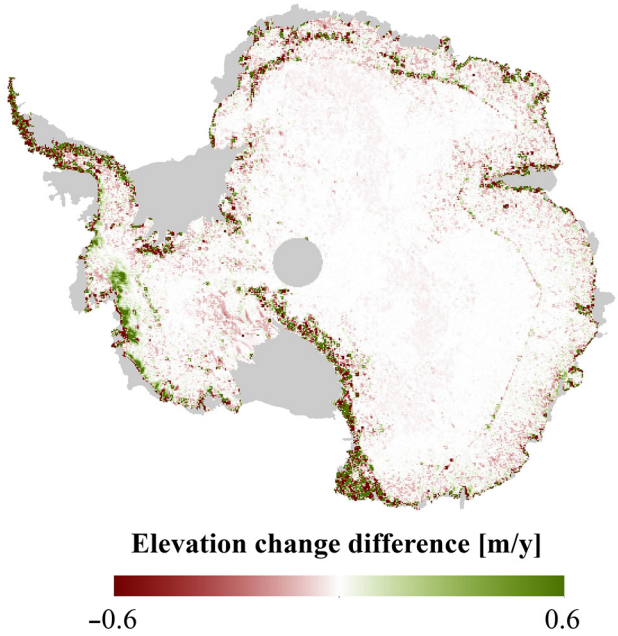

Fig. 4 Difference between the elevation changes from this study and the elevation changes from ICESat-2 data.

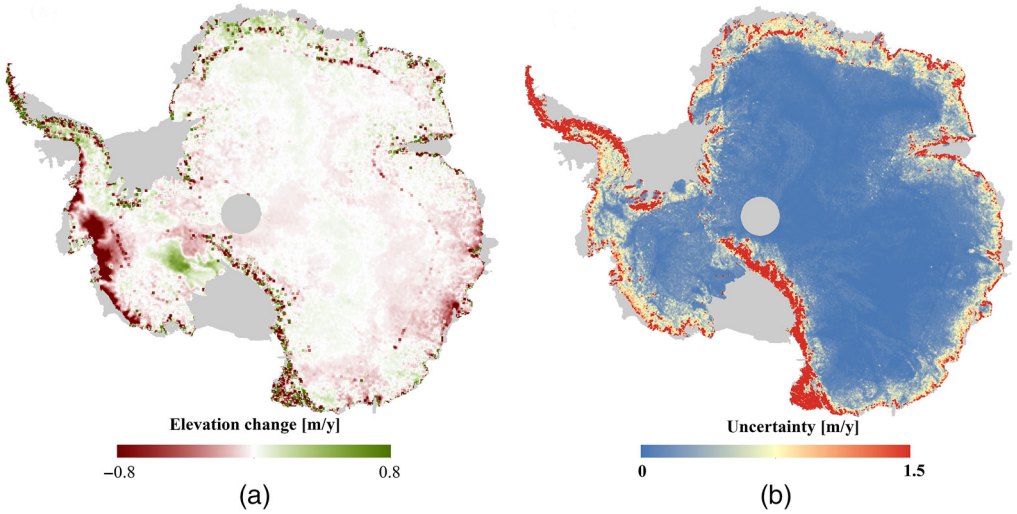

Fig. 5 (a) Antarctic elevation change rates during 2016 to 2019 from joint CryoSat-2 and Sentinel-3 altimeter data and (b) the corresponding uncertainty.

3.3 *Analysis of Elevation Changes in Antarctic Ice Sheet*

The change in the Antarctic ice sheet elevation rates during 2016 to 2019 from the joint CryoSat-2 and Sentinel-3 altimeter data were derived using the process described above. The results are shown in Fig. 5. The southern end of the data range reached 88°S, where the 81.35°S–88°S was obtained from CryoSat-2 data alone. In recent years, areas of rapid ablation remain in the Amundsen Sea and Totten Glacier, reaching an annual lowering rate of several meters. Also similar to the results of earlier studies, the thickening areas of the Antarctic ice sheet were in the Kamb Ice Stream, Dronning Maud Land, and parts of the Antarctic Peninsula.[12,15,16,21] The results of this study yield that the average rate of change in Antarctic ice sheet elevation during 2016 to 2019 was -4.3 ± 0.9 cm/y, with the Antarctic interior changing at -1.1 ± 0.3 cm/y, which was more stable than the margin. In contrast to the instability in the West of Antarctic, the East of Antarctic showed an overall gentle change, with almost all of the East interior elevation change rates <1 cm/y. Combined with the comparison of elevation changes between periods in Fig. 2(a), although the Antarctic ice sheet maintained a relatively small change in elevation rate for most areas, several typical regions of rapid lowering were still accelerating, with increasingly rapid ice loss occurring. Figure 5(b) shows the uncertainty of the Antarctic ice sheet change in elevation rates. The inland ice sheet had a minimal uncertainty of <0.5 m/y, while the uncertainty was >1 m/y on the edge of an unstable ice sheet. Areas with high uncertainty showed the same anomalies in terms of elevation changes in Fig. 5(a). However, not all areas with significant elevation changes had excessive uncertainty. For example, the Pine Island Glacier, which had the most significant elevation decrease, did not have considerable uncertainty. Because the accuracy of radar altimeter measurements is strongly influenced by the topography of the ice sheet surface, the uncertainty depended more on the topographic complexity.

This study shows that Sentinel-3, the new radar altimeter, could be used in combination with altimeters such as CryoSat-2 for monitoring ice sheet elevation changes, and those obtained from these two data sets were reasonable and consistent with previous studies. Although previous studies have proposed the joint application of CryoSat-2 and earlier altimeters, the addition of Sentinel-3 altimeter data would provide longer-term monitoring of ice sheet changes. In the following, this study analyzed the elevation changes of the Antarctic ice sheet in detail based on the results, including the relationship between topographic slope and elevation change rates, statistical analysis of different subregions, and the time series of elevation changes at typical locations.

The Antarctic ice sheet elevation changes have shown significant anomalies in mountainous areas such as those along the Ross Sea and the Antarctic Peninsula, with an inconsistent local trend. These outliers generally occur in regions with large terrain undulation. The areas with

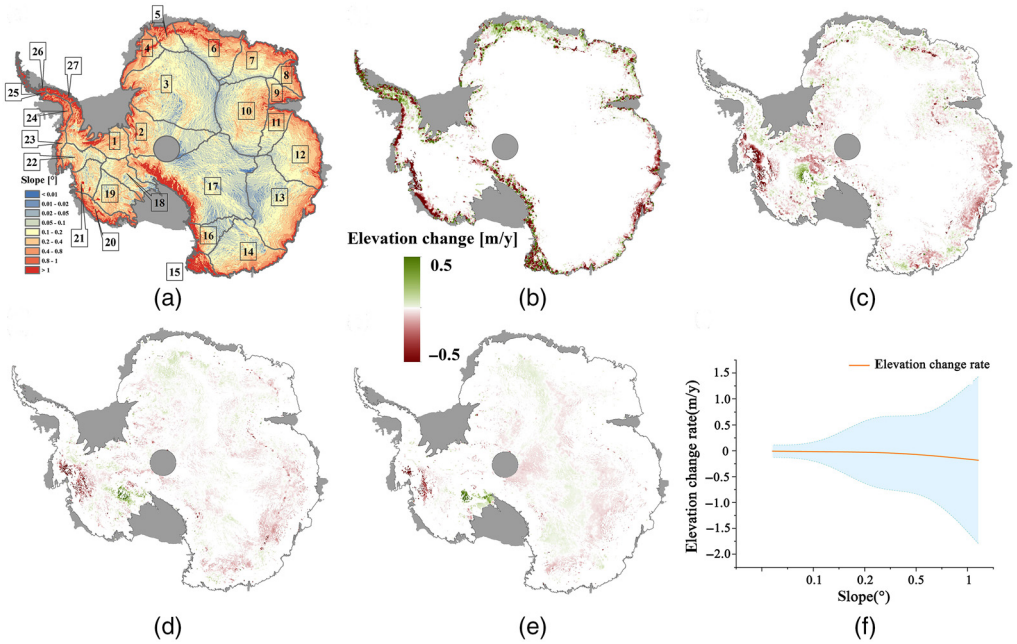

Fig. 6 (a) The surface slope of the Antarctic ice sheet and the division of the 27 drainage systems. (b)–(e) The elevation changes for regions with slopes in the range of >0.5 deg, 0.2 to 0.5 deg, 0.1 to 0.2 deg, and <0.1 deg, respectively. (f) The yellow curve is derived by fitting the elevation change rates with slopes, and the blue area indicates the error range.

significant elevation changes are mainly located in large slope zones. Figure 6(a) shows a schematic of the slope of the Antarctic ice sheet derived by the Reference Elevation Model of Antarctic (REMA), which is provided by The Polar Geospatial Center (PGC) at the University of Minnesota.[47] The two regions with the most irregular rate of change in elevation mentioned above corresponded to the maximum surface slope.

This study mapped the elevation changes of regions with different surface slope ranges. The regions with slopes >0.5 deg [Fig. 6(b)] were mainly located in the mountains or ice shelves at the edge of the ice sheet, and some of these regions showed inconsistent overvalues or undervalues in Fig. 5(a). Such outliers mainly originated from the large uncertainties of radar altimeter measurements. Another part of the region had a generally rapid ice thinning or thickening rate. This part was located at the land-ocean interface, where it was vulnerable to erosion by warm seawater and ice sinking, and ice cracking caused by the Earth's gravity.[48] Both Pine Island Glacier, where rapid lowering occurs, and the Kamb Ice Stream, where ice cover thickening occurs, are located in the 0.2 deg to 0.5 deg slope range [Fig. 6(c)]. Ice sheet elevations on the mid-slope regions were still changing at an above-average rate, and areas in this range greatly impacted the overall ice volume loss. The low-slope regions in Figs. 6(d) and 6(e) covered more than half of the Antarctic ice sheet. Except for a small number of regions in rapid change, 80% of the low-slope regions had a rate in the range of −0.1 to 0.1 m/y. The above analysis shows a correlation between the surface slope and the elevation changes; Fig. 6(f) shows the fitting results. According to the orange curve in the figure, the annual elevation decrease rate varied from <0.1 cm to >10 cm as the slope increased, and the uncertainty of elevation changes (the blue area) also increased substantially with the slope. On the inland ice surface with slope < 0.1 deg, the average change in elevation rate was only -0.007 ± 0.1187 m/y, when the slope increased to the range of 0.1 to 0.2 deg and 0.2 to 0.5 deg, the change in elevation rate also accelerated to -0.0179 ± 0.1295 m/y and -0.0246 ± 0.8132 m/y, respectively. The average change rate in the 0.5 deg to 1 deg range was -0.0778 ± 0.6286 m/y, more than three times the rate in the 0.2 deg to 0.5 deg range. In contrast, the regions beyond 1 deg not only had faster ablations but also presented greater inconsistency of the elevation changes, with an average rate of -0.1819 ± 1.6078 m/y.

The Antarctic continent contains 27 drainage systems,[49] and their division is shown in Fig. 6(a). The three components of the Antarctic continent are formed based on these drainage systems, which are the East Antarctic ice sheet (systems 2 to 17), the West Antarctic ice sheet (systems 1 and 18 to 23), and the Antarctic Peninsula (systems 24 to 27). To further illustrate the terrain features and elevation change characteristics of different regions of the Antarctic ice sheet, this study counted statistics for the three components and 27 drainage systems in Table 5, including their areas, average elevations, slopes, elevation changes, backscatter coefficients, and waveform parameters.

The East Antarctic ice sheet is the largest region, accounting for about two-thirds of the entire Antarctic continent. Most of it is located in the eastern hemisphere, and it is the coldest and driest region on Earth, with an average elevation of over 2000 m. Most of the interior of the East Antarctic ice sheet has a small slope. For example, systems 3, 10, and 13 have an average slope of about 0.2 deg. But the margins are often characterized by steep mountains and ice shelves, with five systems having slopes exceeding 0.5 deg and system 15, primarily occupied by mountains, reaching more than 2 deg. Due to the stability of the large inland ice, the average change in elevation rate in the East Antarctic ice sheet was about -0.032 m/y, which was similar to that of the entire Antarctic ice sheet. The two highest change rates remained in systems 5 and 15, where the slope was the largest, and it was consistent with the analysis of the correlation between slope and elevation change rates above.

The West Antarctic ice sheet experienced the most severe ice loss. It could be divided into three parts, flowing northeastward into the Weddell Sea, westward into the Ross Ice Shelf, and northward into the Amundsen Sea.[50] The average rate of elevation change here was about -0.190 m/y, much greater than that of the East Antarctic ice sheet and the Antarctic Peninsula. As a result, the ice shelves near the Amundsen Sea were experiencing extremely rapid melting. The average elevation change rates in systems 20 to 23 exceeded 0.2 m, and the fastest change rate of -0.480 m/y occurred in system 21, Pine Island Glacier. Also, system 18, containing Marie Byrd Land, was the only system in the West Antarctic ice sheet with an increasing trend of elevation, where the most significant thickening of the Antarctic ice sheet exists.

The Antarctic Peninsula is a relatively long and thin spine alpine style mountain range, which is the fastest-warming region globally and sensitive to climate change.[49,51] The average slope here reaches 2 deg, and the complex topography prevents high accuracy of the satellite altimetry data, so the elevation changes in the Antarctic Peninsula in Fig. 5 were not consistent. This was also evident from the STD of the elevation changes in Table 5, about five times higher than the East and West Antarctic ice sheets. Nevertheless, there was a slight increasing trend in the average elevation changes of this region, and a more pronounced ice thickening occurred in systems 25 to 27.

Four representative areas with different terrain features were selected to analyze their elevation time series over the 4 years.[21,31] Pine Island Glacier and Totten Glacier were the two fastest thinning regions; Kamb Ice Stream showed a thickening trend, while Lake Vostok maintained a stable elevation. As shown in Fig. 7(a), Pine Island Glacier, a giant ice stream with the fastest thinning rate near the Amundsen Sea area, was the region with the greatest impact on Antarctic ice loss. Similar to the previous findings based on other altimeter data, the average change in elevation rates at points A and B near the grounding line were -2.3 ± 0.04 m/y and -2.2 ± 0.04 m/y, respectively, with most points in the region showing several meters of annual elevation decreases. Pine Island Glacier is tectonically vulnerable to rapid collapse and recession and prone to rapid melting at its base, where grounding lines tend to move upward along ice flows.[52] Although studies have shown that the rate of Pine Island Glacier melting has slowed since 2010, it is still thinning at a maximum rate under the influence of geological formations and environmental changes.

Figure 7(b) shows Totten Glacier, another site showing significant ablation and responsible for ice volume loss in the East Antarctic ice sheet. For Totten Glacier, we derived a similar negative growth curve during 2016 to 2019, confirmed in previous studies.[11,53,54] According to the results of this study, the change rate near point 2 was about -1.3 ± 0.02 m/y, and the thinning rate near point 1 was -0.67 ± 0.03 m/y. The decrease of Totten Glacier mainly came from the melting of the bottom due to the influence of ocean heat entering the cavity below the ice shelf, which is caused by the wind-driven warming of deep water through the submarine

Table 5 Statistics of the East and West Antarctic ice sheet, the Antarctic Peninsula, and 27 drainage systems.

Drainage	Area (10^4 km^2)	Elevation (m)		Slope (deg)		Sec (m/y)*		sig0 (dB)*		Lew (milli-bins)*	
		Mean	STD	Mean	STD	Mean	STD	Mean	STD	Mean	STD
East	976.17	2197.78	820.84	0.49	0.54	−0.032	0.515	5.6	3.8	7.1	2.9
West	174.82	1120.02	555.30	0.48	0.45	−0.190	0.530	7.7	3.3	7.6	2.0
Peninsula	22.70	1041.26	558.62	2.00	1.11	0.002	2.353	−0.9	5.9	8.6	1.7
1	46.47	1100.96	611.80	0.54	0.66	0.030	0.310	6.1	4.1	7.9	2.1
2	60.76	2256.04	897.74	0.25	0.31	−0.023	0.327	7.6	2.6	5.6	2.3
3	150.09	2679.98	826.69	0.17	0.19	0.010	0.073	9.5	3.0	5.1	8.2
4	23.97	1478.74	770.07	0.59	0.50	−0.021	0.803	7.4	4.5	7.7	2.2
5	18.47	2083.82	983.20	0.55	0.51	0.106	0.400	7.8	4.9	7.2	2.5
6	59.93	2352.96	1104.50	0.44	0.44	0.022	0.237	6.1	3.8	7.7	1.9
7	49.33	2233.01	946.55	0.41	0.43	−0.009	0.348	5.5	2.9	7.6	2.1
8	16.17	1721.60	752.24	0.57	0.47	−0.020	0.315	5.3	3.4	8.6	1.6
9	14.58	1709.86	829.79	0.53	0.44	−0.023	0.597	4.6	3.9	8.0	2.0
10	89.35	3104.73	685.61	0.19	0.18	−0.012	0.081	6.3	2.4	5.7	2.1
11	25.24	2483.16	930.62	0.33	0.39	−0.020	0.454	7.3	3.5	7.1	2.1
12	72.24	2245.45	842.11	0.34	0.35	−0.061	0.229	5.9	3.1	8.3	1.8
13	110.87	2493.73	829.05	0.23	0.29	−0.066	0.191	4.2	2.1	6.8	2.1
14	71.13	1998.37	679.23	0.29	0.34	−0.029	0.213	3.6	2.3	7.4	2.1
15	12.34	1446.80	677.04	2.01	1.81	−0.277	1.736	−2.1	7.7	8.4	1.7
16	25.83	2128.87	567.70	0.55	1.12	−0.090	1.167	4.0	5.6	6.7	2.4
17	175.88	2747.36	811.25	0.35	0.89	0.002	1.076	6.2	4.8	5.1	2.8
18	25.40	1056.76	704.54	0.21	0.14	0.104	0.201	11.1	2.4	5.7	2.2
19	35.93	1167.58	607.69	0.27	0.26	−0.006	0.081	12.4	2.6	7.0	2.3
20	17.72	1121.58	629.93	0.86	0.57	−0.283	0.990	4.9	4.4	8.6	1.6
21	21.06	1370.69	475.65	0.38	0.70	−0.480	0.818	7.2	3.9	7.4	2.4
22	20.81	1272.39	496.35	0.27	0.25	−0.382	0.580	7.5	2.5	7.5	2.2
23	7.43	750.20	361.15	0.84	0.55	−0.310	0.729	4.4	3.2	8.9	1.4
24	9.90	1126.62	533.99	0.94	0.45	−0.081	0.944	4.6	3.7	8.6	1.5
25	3.50	1019.58	579.48	2.92	1.67	0.809	3.341	−3.8	7.7	8.1	2.0
26	4.14	884.86	575.37	2.53	1.51	−0.572	2.840	−4.4	5.5	8.5	1.7
27	5.15	1133.98	545.63	1.63	0.80	−0.149	2.288	0.0	6.8	9.0	1.4

*The abbreviations indicate elevation change rates (Sec), backscatter coefficients (sig0), and waveform leading-edge widths (Lew). The first three rows show the statistics of the East and West Antarctic ice sheet and the Antarctic Peninsula, respectively, and rows 4 to 30 show the statistics of the 27 drainage systems in Fig. 5(a).

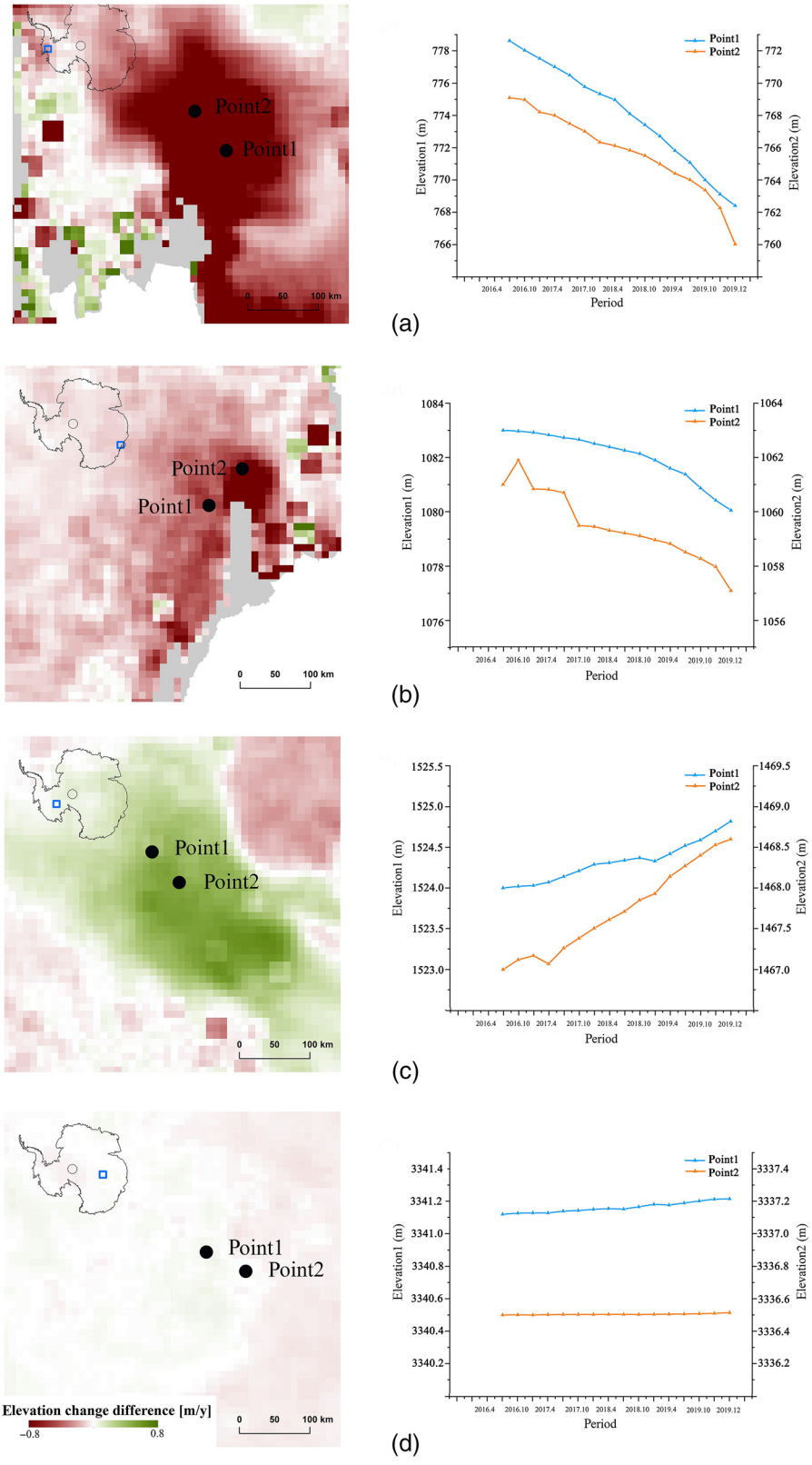

Fig. 7 Elevation time series of (a) Pine Island Glacier, (b) Totten Glacier, (c) Kamb Ice Stream, and (d) Lake Vostok.

canyons into the Totten Ice Shelf cavity.[55,56] Despite minor elevation fluctuations, the overall Totten Glacier elevation has been on a decreasing trend, and changes in this region are essential indicators of global warming.

In Fig. 7(c), the Kamb Ice Stream is located in Marie Byrd Land on the West Antarctic ice sheet. Ice streams are fast-flowing channels within the ice sheet, and ice streams around the Siple coast, including the Kamb Ice Stream, discharge about 40% of the ice from the entire Antarctic ice sheet. These ice streams are important for the stability of the West Antarctic ice sheet.[57,58] Our results show that Kamb Ice Stream has been increasing elevation in recent years, with an average elevation change rate of 0.48 ± 0.01 and 0.65 ± 0.01 m/y at points 1 and 2, respectively. It was one of the fastest thickening regions in the Antarctic continent. Evidence suggests that Kamb Ice Stream was closed a century ago and that its accumulation area is increasing in a negative outflow state. The cessation of the ice flow promoted an overall positive mass balance, and once the nearby Whillans Ice Stream thinned, the ice flow that once discharged into the Kamb Ice Stream began to enter Whillans Ice Stream.[59–61]

Figure 7(d) shows Lake Vostok, a stable area in the Antarctic interior, at an elevation of about 3500 m. It is the largest subglacial lake in the Antarctic, located under the ice in the middle of the East Antarctic ice sheet.[62] Our results show that the elevation change here was very small, with about 0.60 ± 0.08 and 0.20 ± 0.01 cm/y for points 1 and 2, respectively. Although these two points showed a slight increase in elevation, there were also locations in the region with elevation decrease, which was consistent with the conclusions of Schröder et al. and Zhang et al.[21,31]

4 Conclusions

In this study, the latest satellite radar altimeter Sentinel-3 was combined with CryoSat-2 to analyze the surface elevation changes of the Antarctic ice sheet. First, a data filtering method based on subregional clustering was proposed. Two parameters were used to iteratively filter the data according to the surface slopes in different regions. This method removed the outliers in original measurements and improved the accuracy and spatial continuity of the fitting results. Then, an effective fitting method for joint new altimeter data based on the least-squares plane fitting model was proposed to extract the elevation changes during 2016 to 2019. The validation indicated that the results of this study were consistent with the validation data. The results suggest that the new altimeter Sentinel-3 could replace and combine with the previous altimeter to monitor the Antarctic ice sheet changes for a more extended period.

In this study, we analyzed the elevation changes of the Antarctic ice sheet during the 4 years in conjunction with terrain features. The average elevation decreased at a rate of 4.3 ± 0.9 cm/y, while the inner continental ice sheet with flat terrain and simple topography showed a lower decrease rate of 1.1 ± 0.3 cm/y. We derived a correlation between the elevation changes and the surface slope, with rapid elevation changes often occurring in areas with large terrain undulations such as mountainous and marginal ice shelves. We further analyzed the changes in different subdivisions of the Antarctic continent. Three components and the 27 drainage systems were counted. Among them, the East Antarctic ice sheet showed a relatively slow decreasing trend in the average elevation. The flat inland ice sheet was in a very gentle change, and the most severe ablation area in this region was Totten Glacier. The West Antarctic ice sheet was the fastest lowering part, and the Pine Island Glacier was the most severe lowering region with an annual rate of more than 2 m, while the Kamb Ice Glacier was thickening. The Antarctic Peninsula is the most sensitive region to climate change, and its complex topography leads to large uncertainties in elevation changes.

Future monitoring of long-term changes in the Antarctic ice sheet will certainly rely on new satellite radar altimeters. Sentinel-3A/3B, SWOT, and Sentinel-3C/3D satellites in the future will provide significant support in research, and further research will explore the application of these data. A large amount of information in radar signals has not been fully explored in terms of algorithms. Future research will improve signal processing to find more accurate elevation extraction methods by considering ice surface reflection properties and penetration characteristics.

Acknowledgments

This work was supported by the National Natural Science Foundation of China (Grant No. 41871256). Thanks to the organizations that provided data support for this study, the CryoSat-2 altimetry data were provided by the European Space Agency (ESA) Earth Online, the Sentinel-3A altimetry data were provided by The Copernicus Open Access Hub, and the OIB ATM data and the ICESat-2 data were obtained from the National Snow and Ice Data Center (NSIDC). The authors would like to express thanks to the anonymous reviewers for their voluntary work and the constructive comments to improve this manuscript.[63,64] The authors declare no conflict of interest.

References

1. B. Bronselaer et al., "Change in future climate due to Antarctic meltwater," *Nature* **564**(7734), 53–58 (2018).
2. F. S. Paolo, H. A. Fricke, and L. Padman, "Volume loss from Antarctic ice shelves is accelerating," *Science* **348**(6232), 327–331 (2015).
3. H. Konrad et al., "Net retreat of Antarctic glacier grounding lines," *Nat. Geosci.* **11**(4), 258–262 (2018).
4. B. Wouters et al., "Dynamic thinning of glaciers on the Southern Antarctic Peninsula," *Science* **348**(6237), 899–903 (2015).
5. N. R. Golledge et al., "The multi-millennial Antarctic commitment to future sea-level rise," *Nature* **526**(7573), 421–425 (2015).
6. F. Rémy and S. Parouty, "Antarctic ice sheet and radar altimetry: a review," *Remote Sens.* **1**(4), 1212–1239 (2009).
7. H. J. Zwally et al., "Surface elevation contours of Greenland and Antarctic ice sheets," *J. Geophys. Res.: Oceans* **88**(C3), 1589–1596 (1983).
8. J. L. Bamber, "A digital elevation model of the Antarctic ice sheet derived from ERS-1 altimeter data and comparison with terrestrial measurements," *Ann. Glaciol.* **20**, 48–54 (1994).
9. J. Bamber, "Ice sheet altimeter processing scheme," *Int. J. Remote Sens.* **15**(4), 925–938 (1994).
10. C. H. Davis and A. C. Ferguson, "Elevation change of the Antarctic ice sheet, 1995-2000, from ERS-2 satellite radar altimetry," *IEEE Trans. Geosci. Remote Sens.* **42**(11), 2437–2445 (2004).
11. H. D. Pritchard et al., "Extensive dynamic thinning on the margins of the Greenland and Antarctic ice sheets," *Nature* **461**(7266), 971–975 (2009).
12. T. Flament and F. Rémy, "Dynamic thinning of Antarctic glaciers from along-track repeat radar altimetry," *Journal of Glaciology* **58**(211), 830–840 (2012).
13. A. Shepherd et al., "A reconciled estimate of ice-sheet mass balance," *Science* **338**(6111), 1183–1189 (2012).
14. M. McMillan et al., "Increased ice losses from Antarctica detected by CryoSat-2," *Geophys. Res. Lett.* **41**(11), 3899–3905 (2014).
15. V. Helm, A. Humbert, and H. Miller, "Elevation and elevation change of Greenland and Antarctica derived from CryoSat-2," *Cryosphere* **8**(4), 1539–1559 (2014).
16. D. Wingham, "Mass balance of the Antarctic ice sheet," *Philos. Trans. R. Soc. A: Math. Phys. Eng. Sci.* **364**(1844), 1627–1635 (2006).
17. Y. Li and C. H. Davis, "Improved methods for analysis of decadal elevation-change time series over Antarctica," *IEEE Trans. Geosci. Remote Sens.* **44**(10), 2687–2697 (2006).
18. H. A. Fricker and L. Padman, "Thirty years of elevation change on Antarctic Peninsula ice shelves from multimission satellite radar altimetry," *J. Geophys. Res.: Oceans* **117**(C2), C02026 (2012).
19. F. S. Paolo, H. A. Fricker, and L. Padman, "Constructing improved decadal records of Antarctic ice shelf height change from multiple satellite radar altimeters," *Remote Sens. Environ.* **177**, 192–205 (2016).

20. S. Adusumilli et al., "Variable basal melt rates of Antarctic peninsula ice shelves, 1994-2016," *Geophys. Res. Lett.* **45**(9), 4086–4095 (2018).
21. L. Schröder et al., "Four decades of Antarctic surface elevation changes from multi-mission satellite altimetry," *Cryosphere* **13**(2), 427–449 (2019).
22. S. Biancamaria et al., "Satellite radar altimetry water elevations performance over a 200 m wide river: evaluation over the Garonne River," *Adv. Space Res.* **59**(1), 128–146 (2017).
23. M. McMillan et al., "Sentinel-3 delay-Doppler altimetry over Antarctica," *Cryosphere* **13**(2), 709–722 (2019).
24. B. Legrésy, F. Rémy, and F. Blarel, "Along track repeat altimetry for ice sheets and continental surface studies," in *Proc. Symp. 15 Years of Progress in Radar Altimetry*, European Space Agency Publication Division, Noordwijk, The Netherlands (2006).
25. J. Nilsson et al., "Improved retrieval of land ice topography from CryoSat-2 data and its impact for volume-change estimation of the Greenland Ice Sheet," *Cryosphere* **10**(6), 2953–2969 (2016).
26. S. B. Simonsen and L. S. Sørensen, "Implications of changing scattering properties on Greenland ice sheet volume change from CryoSat-2 altimetry," *Remote Sens. Environ.* **190**, 207–216 (2017).
27. D. J. Wingham et al., "Antarctic elevation change from 1992 to 1996," *Science* **282**(5388), 456–458 (1998).
28. H. J. Zwally et al., "Mass gains of the Antarctic ice sheet exceed losses," *J. Glaciol.* **61**(230), 1019–1036 (2015).
29. A. Michel, T. Flament, and F. Rémy, "Study of the penetration bias of ENVISAT altimeter observations over Antarctica in comparison to ICESat observations," *Remote Sens.* **6**(10), 9412–9434 (2014).
30. F. Frappart et al., "An ERS-2 altimetry reprocessing compatible with ENVISAT for long-term land and ice sheets studies," *Remote Sens. Environ.* **184**, 558–581 (2016).
31. B. Zhang et al., "Elevation changes of the Antarctic Ice sheet from joint envisat and CryoSat-2 radar altimetry," *Remote Sens.* **12**(22), 3746 (2020).
32. L. S. Sørensen et al., "Mass balance of the Greenland ice sheet (2003–2008) from ICESat data: the impact of interpolation, sampling and firn density," *Cryosphere* **5**(1), 173–186 (2011).
33. R. K. Raney, "The delay/Doppler radar altimeter," *IEEE Trans. Geosci. Remote Sens.* **36**(5), 1578–1588 (1998).
34. M. McMillan et al., "Three-dimensional mapping by CryoSat-2 of subglacial lake volume changes," *Geophys. Res. Lett.* **40**(16), 4321–4327 (2013).
35. D. Wingham et al., "CryoSat: a mission to determine the fluctuations in Earth's land and marine ice fields," *Adv. Space Res.* **37**(4), 841–871 (2006).
36. C. Bouzinac, "CryoSat product handbook," (2014). https://earth.esa.int/documents/10174/125272/CryoSat_Product_Handbook (accessed on 10 September 2019).
37. C. Donlon et al., "The global monitoring for environment and security (GMES) Sentinel-3 mission," *Remote Sens. Environ.* **120**, 37–57 (2012).
38. W. E. Krabill et al., "Greenland ice sheet: increased coastal thinning," *Geophys. Res. Lett.* **31**(24) (2004).
39. C. F. Martin et al., "*Airborne topographic mapper calibration procedures and accuracy assessment*," NASA Technical Report NASA/TM/u20132012-215891, Goddard Space Flight Center, Greenbelt, Maryland. https://ntrs.nasa.gov/archive/nasa/casi.ntrs.nasa.gov/20120008479.pdf (accessed 9 November 2015).
40. B. Smith et al., *ATLAS/ICESat-2 L3A Land Ice Height, Version 5*, NASA National Snow and Ice Data Center Distributed Active Archive Center, Boulder, Colorado, USA (2021).
41. E. W. Forgy, "Cluster analysis of multivariate data: efficiency versus interpretability of classifications," *Biometrics* **21**, 768–769 (1965).
42. L. Sandberg Sørensen et al., "25 years of elevation changes of the Greenland Ice Sheet from ERS, Envisat, and CryoSat-2 radar altimetry," *Earth Planet. Sci. Lett.* **495**, 234–241 (2018).
43. H. J. Zwally et al., "Mass changes of the Greenland and Antarctic ice sheets and shelves and contributions to sea-level rise: 1992–2002," *J. Glaciol.* **51**(175), 509–527 (2005).

44. U. Strößenreuther, M. Horwath, and L. Schröder, "How different analysis and interpolation methods affect the accuracy of ice surface elevation changes inferred from satellite altimetry," *Math. Geosci.* **52**(4), 499–525 (2020).
45. H. Ewert, A. Groh, and R. Dietrich, "Volume and mass changes of the Greenland ice sheet inferred from ICESat and GRACE," *J. Geodyn.* **59–60**, 111–123 (2012).
46. A. Shepherd et al., "Trends in Antarctic ice sheet elevation and mass," *Geophys. Res. Lett.* **46**(14), 8174–8183 (2019).
47. M. Howat et al., "The reference elevation model of Antarctica," *Cryosphere* **13**(2), 665–674 (2019).
48. J. Scott et al., "Increased rate of acceleration on Pine Island Glacier strongly coupled to changes in gravitational driving stress," *Cryosphere* **3**(1), 125–131 (2009).
49. R. T. Smith and J. B. Anderson, "Ice-sheet evolution in James Ross Basin, Weddell Sea margin of the Antarctic Peninsula: the seismic stratigraphic record," *Bulletin* **122**(5–6), 830–842 (2010).
50. R. Bindschadler, "The environment and evolution of the West Antarctic ice sheet: setting the stage," *Philos. Trans. R. Soc. A: Math. Phys. Eng. Sci.* **364**(1844), 1583–1605 (2006).
51. B. J. Davies et al., "Antarctic Peninsula ice sheet evolution during the Cenozoic Era," *Quat. Sci. Rev.* **31**, 30–66 (2012).
52. I. Joughin and R. B. Alley, "Stability of the West Antarctic ice sheet in a warming world," *Nat. Geosci.* **4**(8), 506–513 (2011).
53. J. Greenbaum et al., "Ocean access to a cavity beneath Totten Glacier in East Antarctica," *Nat. Geosci.* **8**(4), 294–298 (2015).
54. X. Li et al., "Ice flow dynamics and mass loss of Totten Glacier, East Antarctica, from 1989 to 2015," *Geophys. Res. Lett.* **43**(12), 6366–6373 (2016).
55. C. A. Greene et al., "Wind causes Totten Ice Shelf melt and acceleration," *Sci. Adv.* **3**(11), e170168 (2017).
56. E. Rignot et al., "Ice-shelf melting around Antarctica," *Science* **341**(6143), 266–270 (2013).
57. M. R. Bennett, "Ice streams as the arteries of an ice sheet: their mechanics, stability, and significance," *Earth-Sci. Rev.* **61**(3–4), 309–339 (2003).
58. R. B. Alley and R. A. Bindschadler, "The West Antarctic ice sheet and sea-level change," *West Antarctic Ice Sheet: Behav. Environ.* **77**, 1–11 (2001).
59. R. Retzlaff and C. R. Bentley, "Timing of stagnation of Ice Stream C, West Antarctica, from short-pulse radar studies of buried surface crevasses," *J. Glaciol.* **39**(133), 553–561 (1993).
60. I. Joughin and S. Tulaczyk, "Positive mass balance of the Ross ice streams, West Antarctica," *Science* **295**(5554), 476–480 (2002).
61. H. Conway et al., "Switch of flow direction in an Antarctic ice stream," *Nature* **419**(6906), 465–467 (2002).
62. M. J. Siegert, "Antarctic subglacial lakes," *Earth-Sci. Rev.* **50**(1–2), 29–50 (2000).
63. T. W. Armitage, D. J. Wingham, and A. L. Ridout, "Meteorological origin of the static crossover pattern present in low-resolution-mode CryoSat-2 data over central Antarctica," *IEEE Geosci. Remote Sens. Lett.* **11**(7), 1295–1299 (2014).
64. H. J. Zwally et al., "Antarctic and Greenland drainage systems, GSFC cryospheric sciences laboratory," http://icesat4.gsfc.nasa.gov/cryo_data/ant_grn_drainage_systems.php (2012).

Song Li received her BS degree in remote sensing science and technology from Wuhan University, Wuhan, China, in 2019. She is currently pursuing her MS degree in cartography and geographic information system at the Key Laboratory of Digital Earth Science, Aerospace Information Research Institute, Chinese Academy of Sciences (CAS), Beijing, China. Her research interests include microwave data processing and the application of radar altimeter.

Jingjuan Liao received her BS and MS degrees in geosciences from Nanjing University in 1987 and 1990, respectively, and her PhD in geophysics from the Institute of Geophysics, CAS in 1993. Since 1993, she worked on microwave remote sensing applications at several institutes of

CAS as a researcher. Her research interests include microwave scattering model, data processing, and surface parameters estimation.

Lianchong Zhang received his MS degree in natural geography from Hebei Normal University, Shijiazhuang, China, in 2013, and his PhD in signal and information processing from the Institute of Remote Sensing and Digital Earth, CAS, Beijing, China, in 2019. Since 2020, he has been a postdoctoral fellow at the Aerospace Information Research Institute, CAS. His research interests include Earth observation data integrating, management, and sharing.